PERGAMON

International Journal of Heat and Mass Transfer 42 (1999) 3727–3738

International Journal of HEAT and MASS TRANSFER

www.elsevier.com/locate/ijhmt

The effect of Schmidt number on turbulent scalar mixing in a jet-in-crossflow

Guangbin He*, Yanhu Guo, Andrew T. Hsu

University of Miami, Department of Mechanical Engineering, Coral Gables, FL 33124, USA

Received 13 October 1998; received in revised form 5 February 1999

Abstract

The adequacy and accuracy of the constant Schmidt number assumption in predicting turbulent scalar fields in jet-in-crossflows are assessed in the present work. A round jet injected into a confined crossflow in a rectangular tunnel has been simulated using the Reynolds-averaged Navier–Stokes equations with the standard k–ε turbulence model. The principal observation is that the turbulent Schmidt number has a significant effect on the prediction of the species spreading rate in jet-in-crossflows, especially for the cases where the jet-to-crossflow momentum flux ratios are relatively small. A turbulent Schmidt number of 0.2 is recommended for best agreement with experimental data.

1. Introduction

Jet-in-crossflows are extensively used in gas turbine combustors, where jets are arranged around the circumference of combustion chambers to enhance combustion performance in the primary zone and to dilute the hot combustion product exiting the combustor. For modern low-emission gas turbine combustors, the distributions of temperature and species concentration at the combustor exit are important design parameters. Therefore, quantitative predictions of both species and temperature distributions downstream of the jet are required for advanced combustor design.

Many researchers have experimentally studied a single round jet normally into a confined rectangular crossflow. The majority of past experimental work concentrates on trying to understand the flow structures and velocity field of jet-in-crossflows [1–4]. Compared to velocity measurements and flow structure studies, the experimental work on scalar diffusion in jet-in-crossflows are relatively few. Kamotani and Greber [5] studied the scalar diffusion problem using a heated air jet injected into crossflow, where temperature distribution downstream of the jet was measured using hot wire. Sherif and Pletcher [6] measured the temperature field of a heated water jet normally injected into a water tunnel. Vranos and Liscinsky [7] used marker nephelometry to measure the mean concentration in the center plane of a single jet in crossflow; the results were in good agreement with the single-point measurements of Kamotani and Greber [8]. More recently, laser-induced fluorescence has been used to measure the whole flowfield using dye as a scalar tracer. Smith and Mungal [9] used acetone vapor seeded into the jet to acquire quantitative two-dimensional images of the scalar concentration field for a wide range of velocity ratios.

Numerical simulations of the jet-in-crossflow problem include mainly two groups of approaches: the first employs Direct Numerical Simulation (DNS) or Large-Eddy Simulation (LES), and the second uses the

* Corresponding author. Tel.: +1-305-284-4806; fax: +1-305-284-2580.

E-mail address: ghe@coeds.eng.miami.edu (G. He)

0017-9310/99/$ - see front matter
PII: S0017-9310(99)00050-2

Nomenclature

A_j jet exit area
D jet diameter
D_ϕ turbulent diffusion coefficient
G production rate of turbulence kinetic energy,

$$G = \mu_t \frac{\partial U_i}{\partial x_j}\left[\frac{\partial U_i}{\partial x_j} + \frac{\partial U_j}{\partial x_i}\right]$$

H tunnel height
J jet-to-crossflow momentum flux ratio,

$$J = \frac{\int_{A_j} \rho_j V_j^2 \, dA}{\rho_o U_o^2 A_j}$$

P effective pressure
Pe Peclet number
Re Reynolds number, $Re = (\rho U_o D/\mu)$
Sc turbulent Schmidt number
T temperature
U, V, W mean velocity components in Cartesian coordinates
U_o crossflow inlet velocity
V_j jet exit velocity
X, Y, Z Cartesian coordinates
k turbulence kinetic energy
y^+ dimensionless value of y, $y^+ = \rho C_\mu^{0.25} k^{0.5} y/\mu$

Greek symbols
ε dissipation rate of the turbulence kinetic energy
ϕ general dependent variable
μ molecular viscosity
μ_t eddy viscosity
θ non-dimensional temperature
ρ density

Reynolds-averaged approach. Hahn and Choi [10] used DNS to study the flow structure and velocity field of the jet-in-crossflow at very low Reynolds numbers and low jet-to-crossflow momentum flux ratios. Yuan [11] used the LES method to simulate both the velocity field and scalar transport of the Sherif and Pletcher [6] case at reduced Reynolds numbers. Although DNS and LES has shown promising results, they are not at this point employed by the aircraft engine industry in their routine design simulations because of the relatively large computer memory and CPU requirement.

In current design practices, Reynolds-Averaged Navier–Stokes (RANS) computations are most often used for investigation of the velocity and combustion field of gas turbine combustors. Therefore, there is a need for accurate RANS simulations of the jet-in-crossflow problem; both the prediction of velocity field and the scalar field are desired. RANS simulation of the velocity field has been performed by many researchers in the past decades [12–14]. By contrast, numerical simulations of scalar diffusion in jet-in-crossflows are relatively few, and no systematic study of the turbulent Schmidt number effects is available. Chao and Ho [15] used RANS and the standard k–ε model to calculate the temperature field that was experimentally measured by Kamotani and Greber [5], and found no significant changes in the temperature contour patterns when turbulent Schmidt numbers ranging from 0.5 to 0.9 were used. Catalano et al. [16] predicted the scalar field of a flow where the jet impinged on the ceiling wall but did not mention the value or the effect of the turbulent Schmidt number.

Traditionally, a constant turbulent Schmidt number of approximately 0.8 has been used to predict the

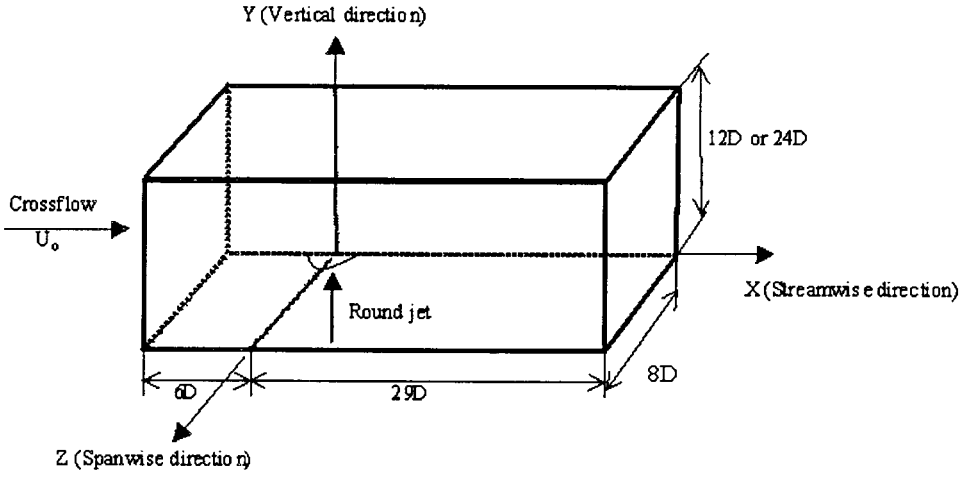

Fig. 1. Flow configuration and coordinate system (symmetric plane $z=0$).

scalar fields of turbulent flows. The objective of the present work is to evaluate the accuracy and limitations of the constant Schmidt number assumption, and to give recommendations on the values of the turbulent Schmidt number that are most suitable for jet-in-crossflow simulations. A semi-empirical analysis on the turbulent Schmidt number is first carried out to suggest a variable turbulent Schmidt number throughout the flow field. A series of RANS simulations, using turbulent Schmidt numbers varying from 0.2 to 1.5, of a confined jet-in-crossflow is performed, wherein turbulence closure is provided by the standard k-ε model [17]. The flow configuration studied in the present work (see Fig. 1) is a round turbulent jet discharging normally into a uniform crossflow in a rectangular tunnel, which was experimentally investigated by Kamotani and Greber [5] and Crabb et al. [1]. The experimental data of Ref. [5] are used to calibrate the selections of turbulent Schmidt numbers, and the experimental data of Ref. [1] is used to validate the numerical observations.

2. Computational approach

2.1. Governing equations

For a variable density incompressible steady flow with constant viscosity, the Reynolds-averaged governing equations for mass, momentum, species concentration, turbulent kinetic energy and its dissipation rate (the standard k–ε model [17]), can be written in the following general form:

$$\frac{\partial}{\partial x_j}(\rho U_j \phi) = \frac{\partial}{\partial x_j}\left(D_\phi \frac{\partial \phi}{\partial x_j}\right) + S_\phi. \tag{1}$$

The detailed equations are specified in Table 1.

In Eq. (1) and Table 1, ϕ is the dependent variable such as velocity, turbulent kinetic energy and its dissipation rate, and species concentration. D_ϕ is the diffusion coefficient.

$$\mu_t = C_\mu \rho k^2/\varepsilon \tag{2}$$

$C_\mu = 0.09$, $c_1 = 1.44$, $c_2 = 1.92$, $\sigma_k = 1.0$, $\sigma_\varepsilon = 1.3$. S represents a scalar such as temperature or species concentration. Sc represents the turbulent Prandtl or Schmidt number.

Since the governing equation for species concentration is identical to the equation for enthalpy if there are no chemical reactions and no external heat source in the physical domain considered, the equation for enthalpy was used throughout the present study, and turbulent Schmidt number and turbulent Prandtl number were not distinguished in the present paper.

Table 1
The detailed governing equations

ϕ	D_ϕ	S_ϕ
1	0	0
U_i, $i=1, 2, 3$	μ_t	$-\partial P/\partial x_i + \partial[\mu_t(\partial U_j/\partial x_i)]/\partial x_j$
S	μ_t/Sc	0
k	μ_t/σ_k	$G-\rho\varepsilon$
ε	μ_t/σ_ε	$(\varepsilon/k)(c_1 G - c_2 \rho\varepsilon)$

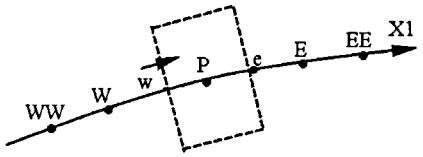

Fig. 2. Computational nodes.

2.2. Numerical schemes

A hybrid differencing scheme and a second-order upwind differencing scheme [18] are used in the discretization of the governing Eq. (1). The computational node locations are shown in Fig. 2. The governing equations are discretized using the finite volume scheme on a given cell, P. In evaluating the fluxes on the cell surfaces, the primitive variable ϕ at a surface (e.g. west surface) of a control volume is calculated using the following scheme

$$\phi_w = \phi_W + \gamma_w(\phi_P - \phi_W)\frac{\phi_W - \phi_{WW}}{\phi_P - \phi_{WW}} \tag{3}$$

where

$$\gamma_w = \begin{cases} 1 & \text{if} \quad |\hat{\phi}_W - 0.5| < 0.5 \\ 0 & \text{otherwise} \end{cases} \tag{4}$$

and

$$\hat{\phi}_W = (\phi_W - \phi_{WW})/(\phi_P - \phi_{WW}). \tag{5}$$

Because the above second-order differencing scheme requires two upstream nodes for each cell-face, which will involve a value outside the solution domain for a near-boundary control volume, the following hybrid scheme was used for all the control volumes adjacent to boundaries

$$\phi_w = \begin{cases} 0.5(\phi_P + \phi_W) & \text{if} \quad Pe \le 2 \\ \phi_W & \text{otherwise} \end{cases} \tag{6}$$

where Pe is the Peclet number, defined as

$$Pe = |C_w/D_w| \tag{7}$$

with C_w representing the mass flux across the west surface and D_w representing the conductance coefficient at the west surface.

The Semi-Implicit Method for Pressure-Linked Equations (SIMPLE) [19] algorithm was used to handle the pressure-velocity coupling. In order to stabilize the solution, under-relaxation factors were used for primitive variables.

2.3. Boundary conditions

A uniform velocity profile at the crossflow inlet was assumed. The velocity profile of a fully-developed turbulent pipe flow was used at the jet inlet boundary. At the inlets of the jet and the crossflow, the turbulence kinetic energy k and its dissipation rate ε are calculated as

$$k = a(U^2 + V^2 + W^2) \tag{8}$$

$$\varepsilon = \frac{C_\mu \rho k^2}{b\mu} \tag{9}$$

where a is a constant, b is the ratio of μ_t/μ. In our calculations, $a = 0.005$ and $b = 100$.

No-slip condition was imposed on the walls, and the standard wall function [17] was used with the standard k–ε model. In this approach, the wall shear stress is related to the flow velocity vector by

$$\vec{\tau}_w = -\lambda_w \vec{V}_p \tag{10}$$

where

$$\lambda_w = \begin{cases} \mu/y_p & \text{if} \quad y_p^+ < 11.6 \\ \rho C_\mu^{0.25} k_p^{0.5} \kappa / \ln(E y_p^+) & \text{otherwise} \end{cases} \tag{11}$$

$$y_p^+ = \rho C_\mu^{0.25} k_p^{0.5} y_p/\mu. \tag{12}$$

In Eqs. (11) and (12), the constants κ and E are 0.41 and 8.432, respectively. The subscript p refers to the first control volume from the wall, and y_p is the normal distance from the wall.

The diffusive flux of turbulence kinetic energy k is zero at the wall, and the near wall values of the production rate G_p and the dissipation rate ε_p are determined from

$$G_p = \tau_w^2/\kappa\mu y_p^+ \tag{13}$$

$$\varepsilon_p = C_\mu^{0.75} k_p^{1.5}/\kappa y_p. \tag{14}$$

A zero gradient condition on all flow variables was imposed at the outflow boundary.

2.4. Flow configuration and grid

The flow configuration used in this work is that of a round turbulent jet normally discharging into a uniform crossflow. In the case of Ref. [1], a turbulent jet was injected normally into a uniform mainstream in a rectangular wind tunnel from a 25.4 mm inside diameter and 0.75 m long pipe. The jet-to-crossflow velocity

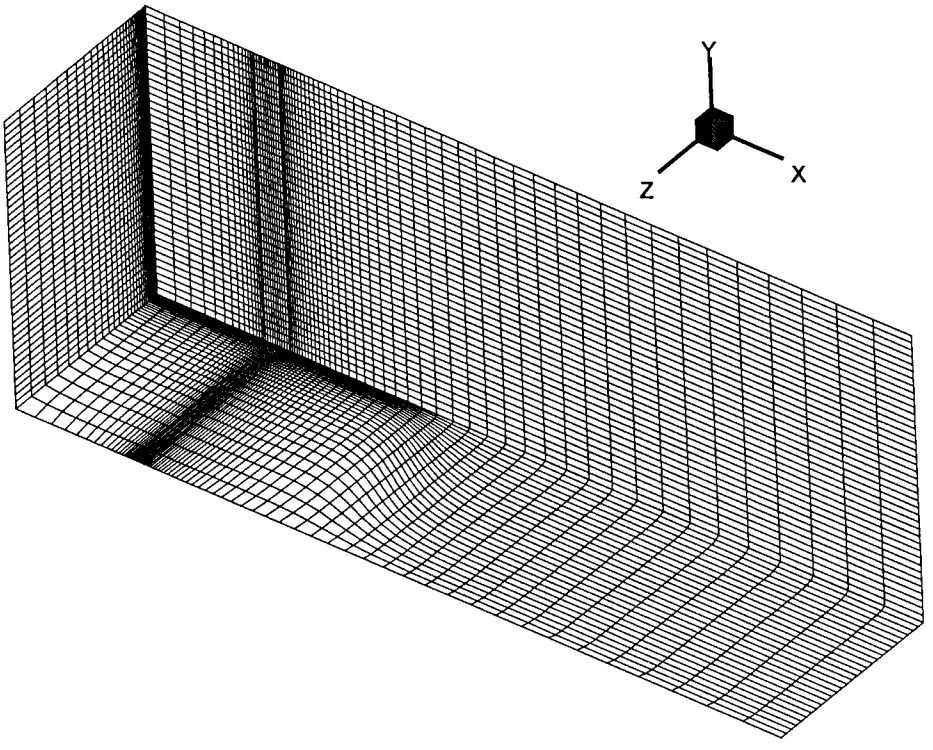

Fig. 3. Structured grid used in the current study.

ratio is 2.3, the crossflow velocity is 12.0 m/s. The Reynolds number based on the crossflow inlet velocity and the jet diameter is about 20,000. The jet and the crossflow have the same temperature. A laser Doppler anemometer (LDA) was used to measure the velocity field. Helium tracer was seeded in the flow field for the measurement of species concentration distribution.

In the case of Ref. [5], a heated round jet was issued normally into a uniform crossflow in a rectangular tunnel. The temperature difference between the jet and the crossflow is 167 K, with the jet temperature at 465 K. Iron-constantan thermocouples were used to measure the temperature distribution. The distance from the jet exit to the ceiling wall is $H=12D$ for momentum flux ratios of $J=8$ and 32, and $H=24D$ for $J=72$. The jet-to-crossflow momentum flux ratio is defined as

$$J=\frac{\int_{A_j}\rho_j V_j^2\,\mathrm{d}A}{\rho_o U_o^2 A_j} \tag{15}$$

where U_o is crossflow inlet velocity, V_j is jet exit velocity, A_j is the jet area, ρ is density, subscripts o and j denote crossflow and jet, respectively. The Reynolds number based on the crossflow inlet velocity and the jet diameter is about 3300.

Based on the symmetry about the jet center plane, the computational domain was established on half the flowfield. The flow geometry and the coordinate system are described in Fig. 1. The jet center is located at $6D$ downstream of the crossflow inlet, which guarantees that the inlet boundary of the crossflow has little effect on the computed flowfield. In order to eliminate any unwanted feedback from the downstream boundary, the tunnel exit is put at $29D$ downstream of the jet. The domain size in the spanwise and the vertical direction are $8D$ and $12D$, respectively. In this computation domain, a nonorthogonal boundary-fitted grid of $90\times45\times40$ was generated in the streamwise, vertical, and spanwise directions, respectively. This selection is the result of a grid independence study, where grid sizes of $50\times40\times30$, $70\times45\times40$, $90\times45\times40$, and $90\times50\times45$ have been tested, together with various stretching factors. The peak velocity in the flow field was compared to check grid independence. As shown in Fig. 3, stretched grids were used along the streamwise and spanwise directions, while uniform grids were used along the vertical direction. Ten uniform grids were selected inside the jet in the streamwise direction as a result of grid independence study. With the selected grid of $90\times45\times40$, the smallest y^+ is about 30, which indicates that the first grid node above the wall is in the logarithmic region of turbulence boundary layer.

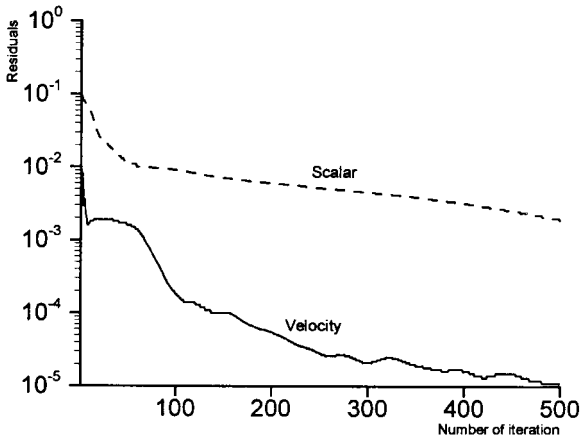

Fig. 4. Error residuals reducing history in the numerical solution.

3. A qualitative analysis for selection of turbulent Schmidt number

Kamotani and Greber [8] established correlations of the velocity and temperature trajectories based on their experimental data:

$$\frac{Y_v}{D} = a_v\left(\frac{X}{D}\right)^{b_v} \tag{16}$$

$$\frac{Y_T}{D} = a_T\left(\frac{X}{D}\right)^{b_T} \tag{17}$$

where y_v and y_T denote vertical coordinates of velocity trajectory and temperature trajectory, respectively; a_v, b_v, b_T are functions of the jet-to-crossflow momentum flux ratio and a_T depends mainly on the momentum flux ratio and weakly on the density ratio. With the momentum flux ratio in the range of 15–60, and the temperature difference in the range of 0–177 K, the above two formulas become

$$\frac{Y_v}{D} = 0.89J^{0.47}\left(\frac{X}{D}\right)^{0.36} \tag{18}$$

$$\frac{Y_T}{D} = 0.73J^{0.52}\left(\frac{\rho_j}{\rho_o}\right)^{0.11}\left(\frac{X}{D}\right)^{0.29} \tag{19}$$

where J is the jet-to-crossflow momentum flux ratio, ρ_j and ρ_o are densities of the jet and the crossflow. One may assume a relation between the turbulent Schmidt number and the trajectories of the velocity and the temperature by using Eqs. (18) and (19):

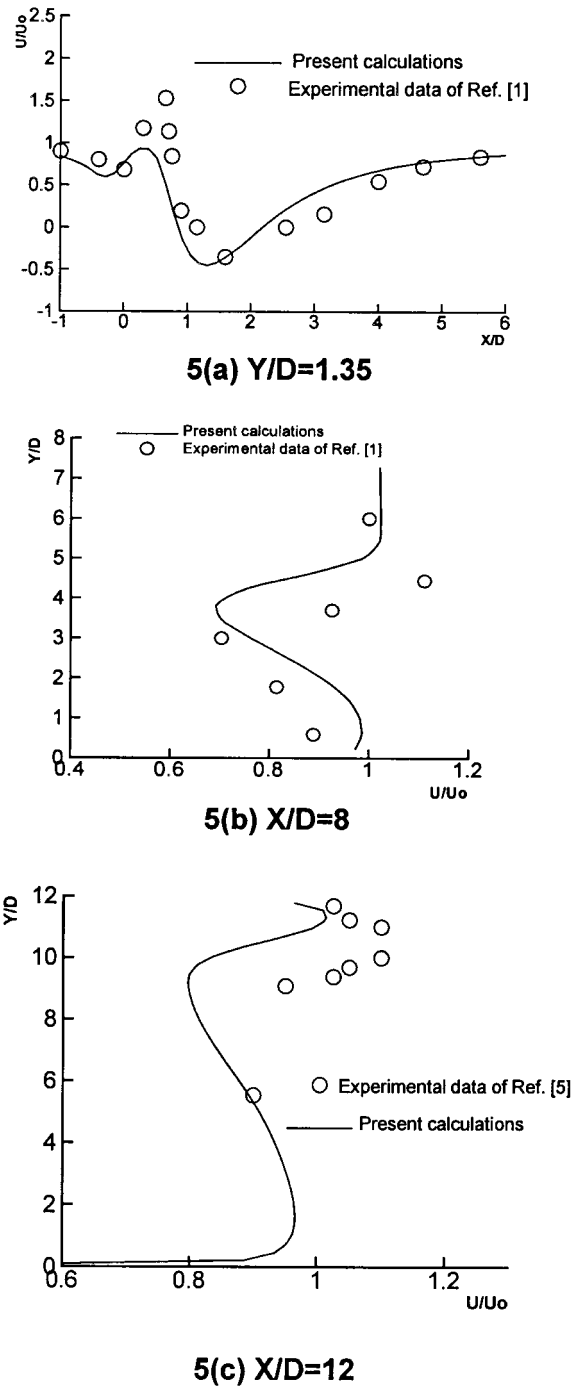

Fig. 5. Streamwise velocities at the jet center plane.

$$Sc = \frac{\nu_t}{D_\phi} \propto \frac{Y_T}{Y_v} = 0.82J^{0.05}\left(\frac{\rho_j}{\rho_o}\right)^{0.11}\left(\frac{X}{D}\right)^{-0.07}. \tag{20}$$

The above empirical relationship indicates that the turbulent Schmidt number increases slightly with increas-

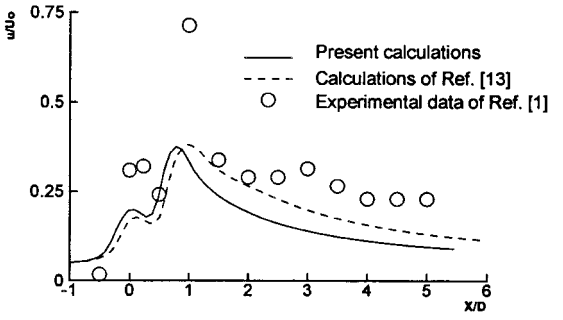

Fig. 6. Turbulence intensity at $y/D=1.35$ and $Z/D=0$.

ing momentum flux ratio and density ratio, and decreases with increasing x/D. This argument suggests that the turbulent Schmidt number be a variable instead of a constant in jet-in-crossflow simulations.

4. Computational results and discussion

In this section, the computed results of mean velocity, turbulence intensity, jet trajectories, and temperature contours are presented. These calculated results are compared with experimental measurements of Refs. [1] and [5]. The recommended turbulent Schmidt number is calibrated against the experimental data of Ref. [5] and then validated by the data of Ref. [1]. The limitations of the constant Schmidt assumption and k–ε model in scalar predictions are discussed.

In all the computations reported in the following, a grid of $90 \times 45 \times 40$ was used and a grid independence study found that further refinement of the grid did not affect the solution. Convergence was determined by monitoring the L2-norm of the flux residuals. To get converged solutions, the residuals dropped at least three orders of magnitude for velocity components and at least two orders for scalar variables. Fig. 4 shows a typical convergence history. Three hundred and fifty iterations were generally required for the cases where turbulent Schmidt numbers are relatively high (greater than 0.5), and 450 or more iterations were required for the low turbulent Schmidt number cases ($Sc=0.2$ and 0.3). A converged solution required approximately 200 μs/iteration/grid-point CPU time on an SGI-OCTANE workstation, and required approximately 350 μs/iteration/grid-point CPU time on an SGI-INDY workstation.

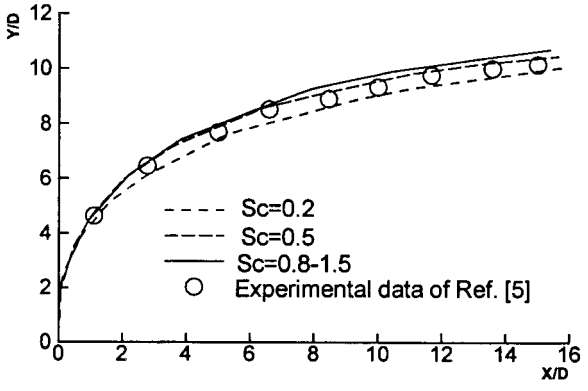

Fig. 7. Effect of turbulent Schmidt number on the prediction of the jet temperature trajectory.

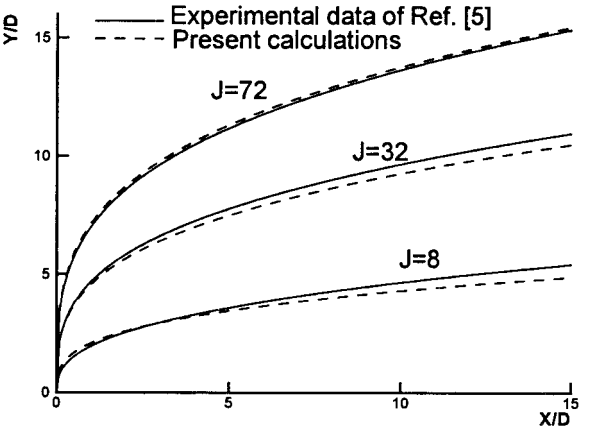

Fig. 8. Jet temperature trajectories between measurements and calculations.

4.1. Mean velocity and turbulence intensity calculations

Comparisons of the calculated velocities with experimental data of Refs. [1] and [5] shown in Fig. 5. Fig. 5(a) presents the streamwise velocity distribution at the jet center plane and $Y=1.35D$, and Fig. 5(b) presents the comparison at the jet center plane and $X=8D$ for the case of Ref. [1]. Fig. 5(c) shows the predicted streamwise velocity at the jet center plane and $X=12D$ for the case of $J=32$, compared to the measured velocity by Ref. [5]. Fig. 6 compares the computed turbulence intensity with experimental data at the jet center plane and $Y=1.35D$ for the case of Crabb et al. The calculated results of Ref. [13], using 2.4 million computational nodes, are also presented in the same figure.

Figs. 5 and 6 show that the velocity fields were reasonably well predicted, but the turbulence intensity was somewhat under-predicted. The discrepancies between numerical predictions and experimental data are believed to be caused by the deficiencies of the standard k-ε model. The standard k–ε model is strictly based on a gradient hypothesis for the turbulent fluxes. Andreopoulos and Rodi [2] had shown experimentally that there is a significant adverse gradient transport in the jet-in-crossflow configuration, which points to the

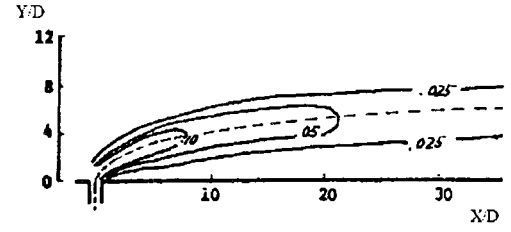

9(a) Experimental data of Ref. [5]

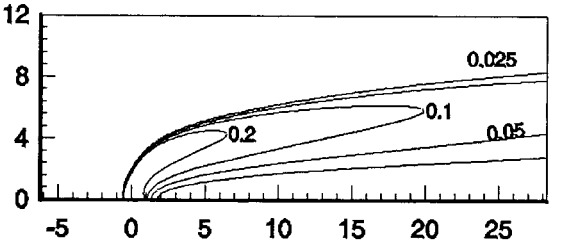

9(d) Sc=0.5

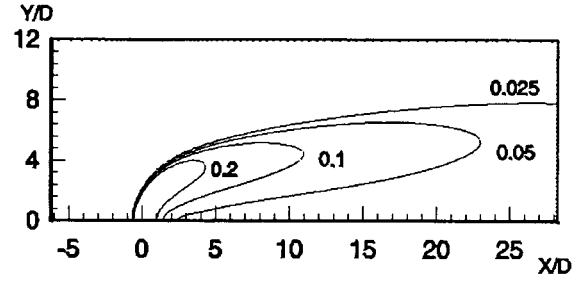

9(b) Sc=0.2

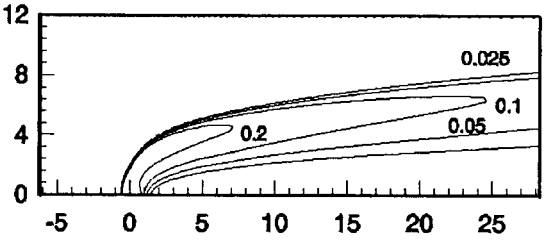

9(e) Sc=0.8

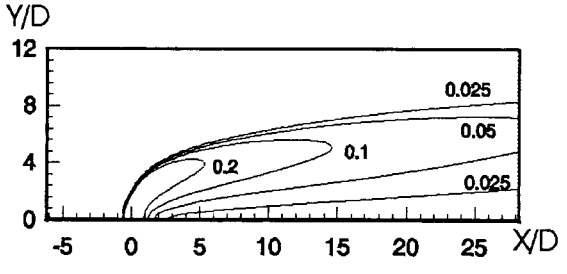

9(c) Sc=0.3

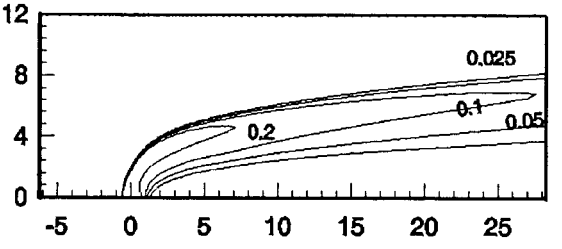

9(f) Sc=1.2

Fig. 9. Fig. 9 Non-dimensional temperature distribution in the symmetric plane ($J=8$, $H/D=12$).

inadequacy of the standard k–ε model in jet-in-crossflow simulations.

4.2. Jet temperature trajectories

Jet trajectory is one of the most important characteristics of jet-in-crossflow problems. The jet temperature trajectory is defined as the locus of the local maximum temperature. The numerically predicted jet trajectories are compared with experimental data of Kamotani and Greber [5] in Figs. 7 and 8. Fig. 7 displays the solutions obtained using various turbulent Schmidt numbers compared with experimental data for the case of $J=32$. The trajectories obtained using turbulent Schmidt numbers ranging from 0.2 to 1.5 all have fairly good agreement with experimental data. Fig. 7 also indicates that while the turbulent Schmidt number has some effects on the prediction of the jet trajectory when it is in the range of 0.2–0.8, the effect is very small for $Sc>0.8$. Fig. 8 shows the predicted

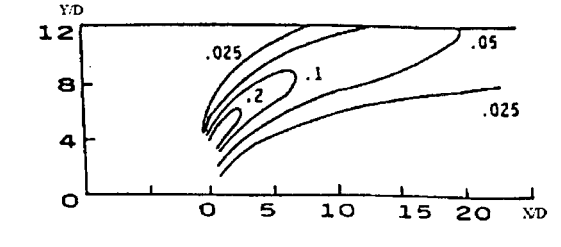

10(a) Experimental data of Ref. [5]

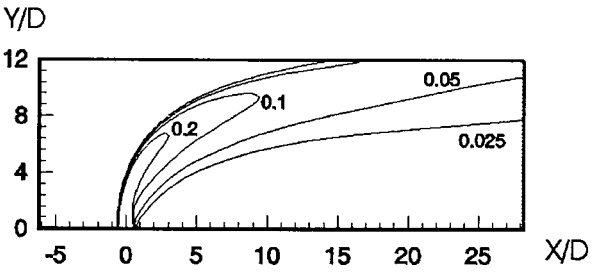

10(d) Sc=0.5

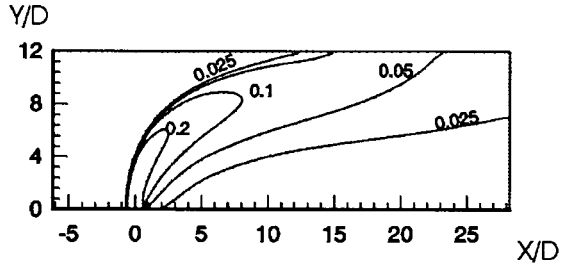

10(b) Sc=0.2

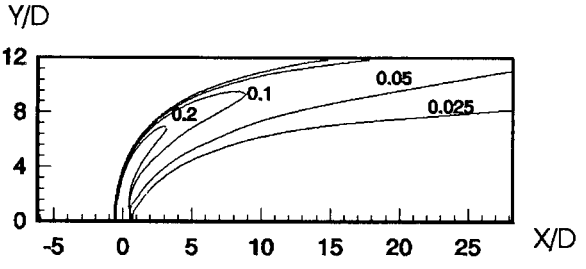

10(e) Sc=0.7

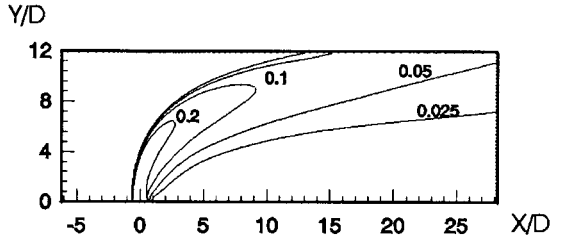

10(c) Sc=0.3

Fig. 10. Non-dimensional temperature distribution in the symmetric plane ($J=32$, $H/D=12$).

jet trajectories using a turbulent Schmidt number of 0.5 for the cases of $J=8$, 32 and 72 compared with the experimental results. General agreement is observed.

4.3. Non-dimensional temperature contours

The temperature was non-dimensionalized by

$$\theta = \frac{T - T_o}{T_j - T_o} \tag{21}$$

where T_j is temperature of the jet and T_o is temperature of the crossflow.

The temperature contours at the jet center plane for various momentum flux ratios are compared with experimental data in Figs. 9–11.

4.3.1. Momentum flux ratio J = 8

Turbulent Schmidt numbers 0.2, 0.3, 0.5, 0.8, and 1.2 were tested to study the effects of the Schmidt number on the jet mixing in the crossflow for the case of $J=8$.

Fig. 9 exhibits a quantitative comparison of the predicted temperature contours with experimental measurements. Fig. 9(a) presents the experimental measurements of the temperature distribution in the jet center plane, and Figs. 9(b)–10(f) are numerical results from various turbulent Schmidt numbers. These results indicate that the temperature profiles become slenderer with increasing the turbulent Schmidt number. For example, the contour line of $\theta=0.1$ was predicted to be $X=10D$ downstream of the jet exit when a turbu-

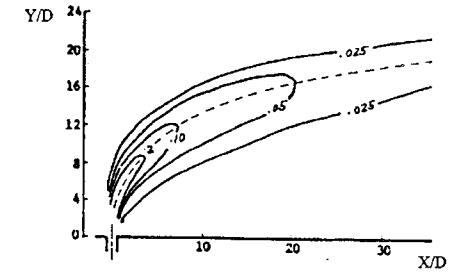

11(a) Experimental data of Ref. [5]

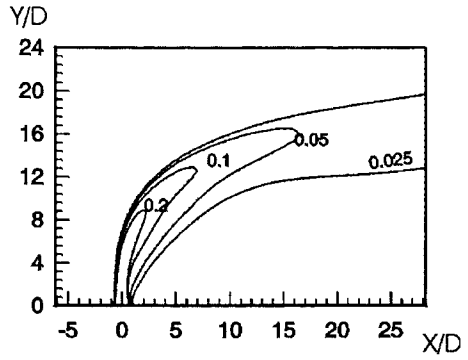

11(d) Sc=0.5

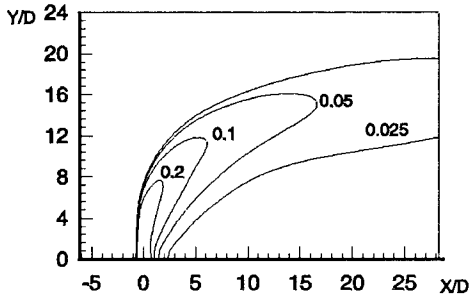

11(b) Sc=0.2

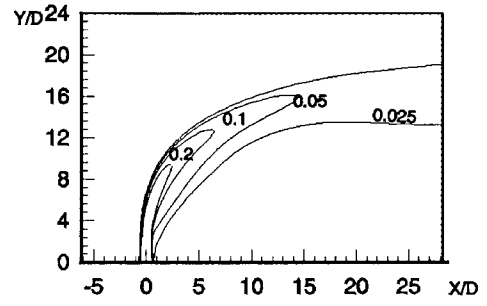

11(e) Sc=0.8

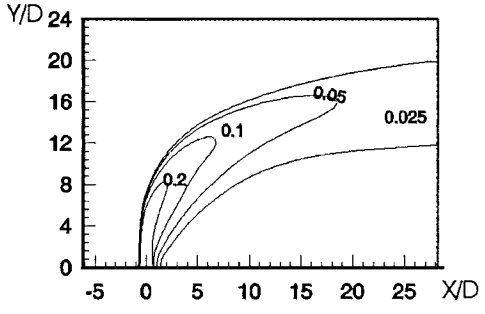

Fig. 11. Non-dimensional temperature distribution in the symmetric plane ($J=72$, $H/D=24$).

lent Schmidt number of 0.2 was used (Fig. 9(b)), while as shown in Fig. 9(d), the location of the contour line of $\theta=0.1$ extended to $X=20D$ when a turbulent Schmidt number of 0.5 was used. The jet mixing rate was found to be quite sensitive to the change in turbulent Schmidt number for this low momentum flux ratio; the predicted temperature field changes substantially with the turbulent Schmidt number. In fact, when the turbulent Schmidt number is greater than 0.3, the agreement between predicted and measured temperature fields become poor.

It should be noted that although the best agreement with experimental data is obtained with $Sc=0.2$, the agreement with experimental data is far from perfect. For instance, the lower part of the contour line of $\theta=0.025$, observed in the experimental data as shown in Fig. 9(a), was not resolved in the prediction using $Sc=0.2$ (Fig. 9(b)). An increase or decrease in the turbulent Schmidt number from the 0.2 value will improve the temperature prediction in some regions but worsen it in others. This indicates that, for low jet-to-crossflow momentum flux ratios, the assumption of a constant Schmidt number may not be the best choice for the jet-in-crossflow problem, and more sophisticated approaches may be required.

4.3.2. Momentum flux ratio J = *32*

Turbulent Schmidt numbers tested for the case of

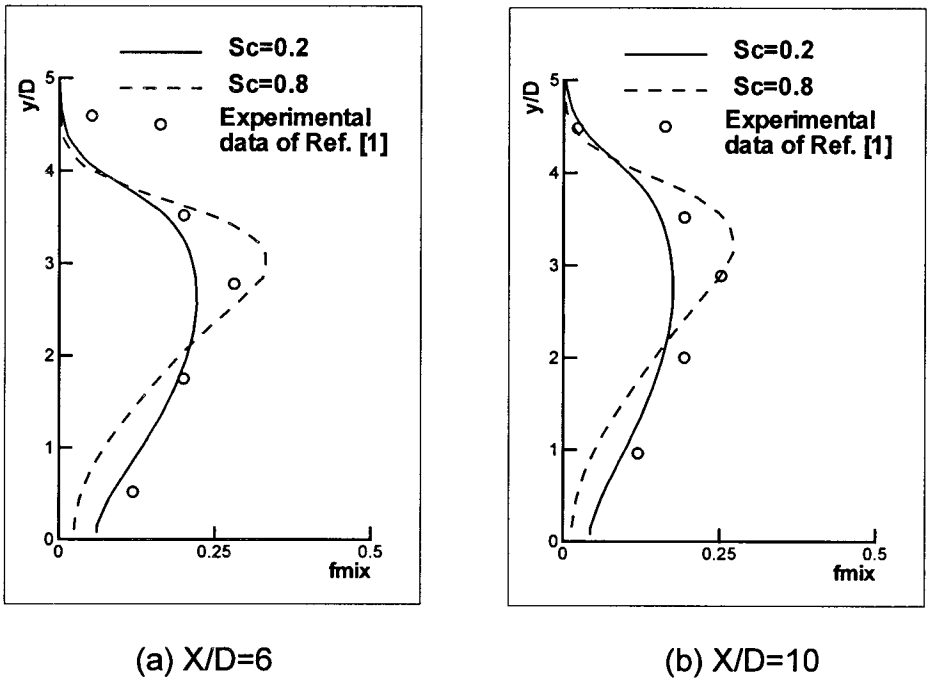

Fig. 12. Species concentration distribution at the jet center plane.

$J=32$ were $Sc=0.2$, 0.3, 0.5, and 0.7. Fig. 10(a) presents the experimental measurements, and Fig. 10(b)–(e) exhibit numerical results from various turbulent Schmidt numbers. In this case, the jet impinged upon the ceiling wall at the downstream of the jet. Generally, a turbulent Schmidt number of 0.2 still gives the best agreement with experimental data. The jet scalar spreading rate is under-predicted with turbulent Schmidt numbers greater than 0.3, but the change is less significant than in the case of $J=8$. Compared to the case of $J=8$, the present results at $Sc=0.2$ show much better agreement with experimental data.

4.3.3. Momentum flux ratio J = *72*

Turbulent Schmidt numbers 0.2, 0.3, 0.5, and 0.8 were used in the case of $J=72$. Results are presented in Fig. 11. It can be seen that the temperature field is quite accurately predicted at $Sc=0.3$. A close examination of Fig. 11 shows that the numerical results from $Sc=0.2$ also compare favorably with the experimental data of the temperature field, although scalar diffusion is slightly over-predicted.

A comparison of Figs. 9–11 shows that the change in temperature distribution for $J=72$ with different Schmidt numbers is far less drastic compared to the cases of $J=8$ and 32. For the relatively high momentum flux ratio of $J=72$, the predicted temperature contours compare much better with experimental data than the two previous cases. One may conclude from this observation that the higher the jet-to-crossflow momentum flux ratio, the less sensitive is the solution to turbulent Schmidt number. One may also conclude that the constant Schmidt number assumption is a reasonable one for jet-in-crossflows of high jet-to-crossflow momentum flux ratios, but less so for those of low momentum flux ratios.

4.4. Validation

In the preceding section, it is recognized that the scalar (temperature) prediction obtained using a value of turbulent Schmidt number of 0.2 best matches the experimental data. To further verify the observation, another set of experimental data obtained by Crabb et al. [1] are used and again used $Sc=0.2$ to calculate the scalar field in a jet-in-crossflow. In this case, Crabb et al. used Helium trace to identify the species concentration distribution in the flow field. Fig. 12 presents the comparison between measured and calculated species concentrations using values of turbulent Schmidt number of 0.2 and 0.8 at two downstream locations of $X/D=6$ and 8. It can be seen that the predicted species concentration profiles using $Sc=0.2$ better match the measured data.

5. Concluding remarks

RANS simulations of the turbulent scalar diffusion process in jet-in-crossflows were performed to evaluate the accuracy of constant Schmidt number assumption and the effect of the turbulent Schmidt number on the mixing of jet species with the crossflow within the context of the standard k–ε model. Good prediction of the jet trajectories and reasonable prediction of the velocity field were obtained. Calculations showed underpredicted turbulence intensity, which indicates that the standard k–ε model does not capture all the important flow physics in jet-in-crossflows.

The turbulent Schmidt number in the range of 0.2–0.8 has some effects on the prediction of the jet trajectory. The effect is very small when the turbulent Schmidt number is larger than 0.8. A significant effect of the turbulent Schmidt number on the prediction of the jet species spreading rate in the jet-in-crossflow was observed, especially so for cases where the jet-to-crossflow momentum flux ratios are relatively small. The most suitable turbulent Schmidt numbers for cases of $J=8$, 32, and 72 were found to be $Sc=0.2$, 0.2, and 0.3, which are considerably smaller than the values that are conventionally used in turbulent combustion simulations. By validation, a turbulent Schmidt number of 0.2 is recommended for jet-in-crossflow simulations because, under the constant Schmidt assumption, it gives the most satisfactory solutions for a wide range of jet-to-crossflow momentum flux ratios.

The constant Schmidt number assumption provides fairly accurate solutions of turbulent scalar mixing for jet-in-crossflow cases where the jet-to-crossflow momentum flux ratios are relatively high, while for low momentum flux ratio jet-in-crossflows a constant Schmidt number may not necessarily be the best choice. The authors' semi-empirical analysis, based on the experimental observations of Kamotani and Greber, shows that the turbulent Schmidt number is dependent on the jet-to-crossflow momentum flux ratio, density ratio, and geometric location. From these observations one may conclude that a variable turbulent Schmidt number is needed for low momentum flux ratio jet-in-crossflows.

Acknowledgements

The authors would like to thank Drs Andreja Brankovic and Saadat Syed from Pratt & Whitney, and Dr N.-S. Liu from NASA Lewis Research Center for their guidance, as well as financial support on this research project.

References

[1] D. Crabb, D.F.G. Durao, J.H. Whitelaw, A round jet normal to a crossflow, Transactions of the ASME, Journal of Fluids Engineering 103 (1981) 142–153.
[2] J. Andreopoulos, W. Rodi, Experimental investigation of jets in a crossflow, Journal of Fluid Mechanics 138 (1984) 93–127.
[3] T.F. Fric, A. Roshko, Vortical structure in the wake of a transverse jet, Journal of Fluid Mechanics 279 (1994) 1–47.
[4] R.M. Kelso, T.T. Lim, A.E. Perry, An experimental study of round jets in crossflow, Journal of Fluid Mechanics 306 (1996) 111–114.
[5] Y. Kamotani, I. Greber Experiments on confined turbulent jets in crossflow. NASA CR-2392 1974.
[6] S.A. Sherif, R.H. Pletcher, Measurements of the thermal characteristics of heated turbulent jets in crossflow, Journal of Heat Transfer 111 (1989) 897–903.
[7] A. Vranos, D.S. Liscinsky, Planar imaging of jet mixing in crossflow, AIAA Journal 26 (1988) 1297–1298.
[8] Y. Kamotani, I. Greber, Experiments on a turbulent jet in a cross flow, AIAA Journal 10 (1972) 1425–1429.
[9] S.H. Smith, M.G. Mungal, Mixing, structure and scaling of the jet in crossflow, Journal of Fluid Mechanics 357 (1998) 83–122.
[10] S. Hahn, H. Choi, Unsteady simulation of jets in a cross flow, Journal of Computational Physics 134 (1997) 342–356.
[11] L.L. Yuan, Large eddy simulations of a jet in crossflow. PhD dissertation, Stanford University 1997.
[12] S.V. Patankar, D.K. Basu, S.A. Alpay, in: Prediction of the three-dimensional velocity field of a deflected turbulent jet, Transactions of the ASME, Journal of Fluid Engineering, 1977, pp. 758–762.
[13] R.W. Claus, S.P. Vanka, Multigrid calculations of a jet in crossflow, Journal of Propulsion and Power 8 (1992) 425–431.
[14] S-W. Kim, T.J. Benson, Calculation of a circular jet in crossflow with a multiple-time-scale turbulence model, Journal of Heat and Mass Transfer 35 (1992) 2357–2365.
[15] Y-C. Chao, W-C. Ho, Heterogeneous and non-isothermal mixing of a lateral jet with a swirling crossflow, Journal of Thermophysics 5 (1990) 394–400.
[16] G.D. Catalano, K.S. Chang, J.A. Mathis, Investigation of turbulent jet impingement in a confined crossflow, AIAA Journal 27 (1989) 1530–1535.
[17] B.E. Launder, D.B. Spalding, The numerical computation of turbulent flows, Computer Methods in Applied Mechanics and Engineering 3 (1974) 269–289.
[18] J. Zhu, A low diffusive and oscillation-free convection scheme, Communications in Applied Numerical Methods 7 (1991) 225–232.
[19] S.V. Patankar, D.B. Spalding, A calculation procedure for heat, mass and momentum transfer in three-dimensional parabolic flows, International Journal of Heat and Mass Transfer 15 (1972) 1778–1806.